Methods

Hierarchical statistical modeling of xylem vulnerability to cavitation

Kiona Ogle[1,2], Jarrett J. Barber[2], Cynthia Willson[3] and Brenda Thompson[2]

[1]Department of Botany and [2]Department of Statistics, University of Wyoming, Laramie, WY 82071, USA; [3]Department of Biology, Duke University, Durham, NC, USA

Summary

Author for correspondence:
Kiona Ogle
Tel: +1 307 766 3219
Fax: +1 307 766 2851
Email: kogle@uwyo.edu

• Cavitation of xylem elements diminishes the water transport capacity of plants, and quantifying xylem vulnerability to cavitation is important to understanding plant function. Current approaches to analyzing hydraulic conductivity (K) data to infer vulnerability to cavitation suffer from problems such as the use of potentially unrealistic vulnerability curves, difficulty interpreting parameters in these curves, a statistical framework that ignores sampling design, and an overly simplistic view of uncertainty.

• This study illustrates how two common curves (exponential-sigmoid and Weibull) can be reparameterized in terms of meaningful parameters: maximum conductivity (k_{sat}), water potential ($-P$) at which percentage loss of conductivity (PLC) = X% (P_X), and the slope of the PLC curve at P_X (S_X), a 'sensitivity' index.

• We provide a hierarchical Bayesian method for fitting the reparameterized curves to K_H data. We illustrate the method using data for roots and stems of two populations of *Juniperus scopulorum* and test for differences in k_{sat}, P_X, and S_X between different groups.

• Two important results emerge from this study. First, the Weibull model is preferred because it produces biologically realistic estimates of PLC near $P = 0$ MPa. Second, stochastic embolisms contribute an important source of uncertainty that should be included in such analyses.

Introduction

Xylem cavitation is one of the primary processes causing reduced water transport capacity in vascular plants (Sperry, 2000), negatively affecting plant carbon balance (Boyer, 1976; Cowan, 1982). When a water-filled conduit is under tension during drought stress, the tension may induce an embolism event whereby the conduit becomes air-filled (Zimmermann, 1983; Tyree & Sperry, 1989) and can no longer function in water transport (Zimmermann, 1983). Hence, cavitation reduces hydraulic conductivity (Sperry, 2000) and can lead to stomatal closure (Sperry & Pockman, 1993), reduced gas exchange (Sperry *et al.*, 1998), and plant mortality (Tyree & Sperry, 1988; Martínez-Vilalta & Piñol, 2002).

A 'vulnerability curve' describes the vulnerability of a plant to xylem cavitation in terms of the percentage loss of hydraulic conductivity (PLC) as a function of xylem water potential (–P) (Tyree & Sperry, 1988). Vulnerability curves provide insight into drought tolerance (Linton *et al.*, 1998; Kolb & Sperry, 1999) and generally capture the range of water potentials experienced in the field (Brodribb & Hill, 1999; Hacke *et al.*, 2000; Pockman & Sperry, 2000). Advances in experimental methodology have yielded a variety of methods for measuring hydraulic conductivity under a range of water potentials (Sperry *et al.*, 2003), ranging from fairly simple and easy-to-implement approaches (Sperry & Sullivan, 1992) to sophisticated techniques that require specialized equipment (Sperry & Saliendra, 1994; Pockman *et al.*, 1995). Novel approaches continue to emerge for measuring vulnerability to

cavitation of small xylem areas (Mayr & Cochard, 2003), sapwood sections (Kikuta *et al.*, 2003), and whole leaves (Brodribb & Holbrook, 2003). Additionally, faster methods are being developed for measuring hydraulic conductivity in tandem with the centrifuge method (Li *et al.*, 2008). On the other hand, statistical methods for analyzing data obtained via these methods are comparatively underdeveloped.

A common procedure for generating a vulnerability curve begins in the laboratory by making several measurements of hydraulic conductivity on a stem or root segment that is subjected progressively to more negative xylem pressures (Sperry & Sullivan, 1992; Sperry & Saliendra, 1994; Pockman *et al.*, 1995). Then, PLC is calculated by comparing hydraulic conductivity measured at each water potential to a potential maximum value that is typically obtained after flushing the segment to remove native emboli (Sperry *et al.*, 1988). However, even at low (positive) pressures, flushing can cause a decrease in conductivity in some angiosperms (Wang *et al.*, 1992; Macinnis-Ng *et al.*, 2004) and conifers (Sperry & Tyree, 1990). Additionally, if the flushing pressure is too low or the time period is too short, dissolution of emboli may be incomplete. Consequently, if all emboli are not removed, then maximum hydraulic conductivity will be underestimated, biasing the resulting vulnerability curve such that PLC at different water potentials will also be underestimated. These issues call for a statistical approach that explicitly accounts for uncertainty in maximum hydraulic conductivity.

Several biologically meaningful parameters have been derived from the theoretical PLC curve. These parameters depict one of two drought-tolerance characteristics: (i) susceptibility to cavitation at a particular *P*; and (ii) sensitivity of cavitation to changes in *P*. The water potential that results in PLC = 50% ($-P_{50}$) is the most commonly used parameter for comparing susceptibility (Tyree & Ewers, 1991). A number of similar parameters have been explored, including the mean cavitation pressure (Sperry & Saliendra, 1994), the air-entry potential (Sparks & Black, 1999; Domec & Gartner, 2001), the 'full embolism' potential (Domec & Gartner, 2001), and P_{75} and P_{100} (Hacke & Sperry, 2001). Sensitivity (*S*) is an important cavitation index and is represented by the slope of the PLC curve at a particular *P*. A plant with a shallow slope experiences gradual loss of conductivity over a wide range of *P* values, while one with a steep slope undergoes rapid cavitation over a small range of *P* values (Sperry, 1995), potentially indicating that the conduit anatomy consists of cells with similar air-seeding vulnerability. Although sensitivity indices have been derived (Pammenter & Vander Willigen, 1998), they are seldom used for comparison. Moreover, while these parameters are indispensable for quantifying and comparing drought-tolerance traits, the estimation procedures that have been applied have not estimated these parameters directly and have employed post-hoc calculations of the parameters that do not provide accurate estimates of their uncertainty.

Different functional forms have been employed to describe a vulnerability curve, including the exponential-sigmoid (Pammenter & Vander Willigen, 1998), the Weibull (Rawlings & Cure, 1985; Neufeld *et al.*, 1992), the Gompertz (Mencuccini & Comstock, 1997), and polynomial functions (Pockman & Sperry, 2000; Jacobsen *et al.*, 2007). All of these models have been utilized to estimate susceptibility parameters (e.g. P_{50}). Pammenter & Vander Willigen (1998) put forth the exponential-sigmoid as an attractive model because it is the only one whose parameters inherently reflect both P_{50} and *S*. However, the purportedly 'linearized' form that they give is, in fact, nonlinear with respect to the parameters (see section 1.2 in Seber & Wild, 1989), typically requiring linear approximations to infer P_{50} and *S*. In this paper, we describe a Bayesian approach to fitting nonlinear vulnerability curves to hydraulic conductivity data that does not require linear approximations to infer P_{50} and *S*. In doing so, we focus on two commonly applied models (i.e. exponential-sigmoid and Weibull) and show that both models can be reparameterized in terms of susceptibility (P_X) and sensitivity (S_X) parameters. Although the reparameterized models are highly nonlinear, Bayesian statistical methods for fitting these models can be implemented in readily available software packages.

Current methods for analyzing data on vulnerability to cavitation are insufficient for capturing the error structure. Most sampling schemes result in several conductivity measurements for an individual segment, and a common approach is to fit separate curves to PLC data for each segment or for a collection of segments (e.g. multiple stems excised from one tree). The point estimates of, for example, P_{50} for each fitted curve are treated as 'data' and an analysis of variance (ANOVA) of these point estimates may be performed with subsequent inference about differences between treatment groups. The observed significance levels (*P*-values) are very likely overly optimistic because of the failure to account for variability of the segment-level estimates of P_X. Frequently, the sampling design suggests a hierarchical structure composed of random and fixed effects (e.g. multiple measurements on a segment, several segments from a tree, many trees within a species, etc.), yet explicit modeling of this dependence structure is absent from previous studies. Such issues are not unique to vulnerability curve analyses, and more rigorous methods have been advocated for physiological response functions in general (Potvin *et al.*, 1990; Peek *et al.*, 2002; Ogle & Barber, 2008).

A primary objective of this study is to provide a statistically rigorous method for analyzing hydraulic conductivity data, comparing different vulnerability curve models, and making subsequent inferences about xylem vulnerability to cavitation. The contributions of the methodology detailed in this study include: incorporation of hierarchical error structures dictated by the experimental or sampling design; explicit representation of process error introduced by stochastic embolism events; quantification of uncertainty in parameter estimates, including maximum hydraulic conductivity; a hierarchical Bayesian

Table 1 Original and reparameterized vulnerability curves for hydraulic conductivity

	Original hydraulic conductivity equations[a]	
Exponential-igmoid	$k = k_{sat}\left\{1 - \dfrac{1}{1 + \exp(a(P - b))}\right\}$	(Eqn 1.1)
Weibull	$k = k_{sat}\exp\left\{-\left(\dfrac{P}{\alpha}\right)^{\beta}\right\}$	(Eqn 1.2)
	Reparameterized hydraulic conductivity equations[a,b]	
Exponential-igmoid	$k = k_{sat}\left\{1 - \dfrac{1}{1 + \left(\dfrac{100}{X} - 1\right)\exp\left(\dfrac{100 S_X (P - P_X)}{X(X - 100)}\right)}\right\}$	(Eqn 1.3)
Weibull	$k = k_{sat}\left(1 - \dfrac{X}{100}\right)^{\left[\left(\dfrac{P}{P_X}\right)^{\frac{P_X S_X}{V}}\right]}$ $V = (X - 100)\ln\left(1 - \dfrac{X}{100}\right)$	(Eqn 1.4)

[a]P is (positive-valued) xylem water potential (i.e. $P = -\Psi$). Equations for k are only provided, and the *plc* equations are easily derived from Eqn 1.
[b]The reparameterized models have three parameters that share the same meaning across models: k_{sat}, saturated hydraulic conductivity, or k at $P = 0$ MPa; P_X, pressure at $X\%$ loss of conductivity; and S_X, the slope of the *plc* curve at $P = P_X$.

modeling framework that accommodates such uncertainty; and reparameterized exponential-sigmoid and Weibull models that explicitly contain meaningful drought-tolerance parameters. We illustrate our methodology using hydraulic conductivity data collected for roots and stems of *Juniperus scopulorum* Sarg. (Rocky Mountain juniper). These statistical methods give parameter estimates that are appropriate to the data and sampling design, thereby aligning the analysis approaches with well-developed laboratory methods.

Description of modeling approach

Vulnerability models reparameterized

Current approaches fit vulnerability curves to PLC data as a function of xylem water potential, a negative-valued tension that is usually expressed as a positive-valued pressure (P). The PLC values are calculated as PLC = $[(K_{max} - K)/K_{max}] \times 100\%$, where K is measured hydraulic conductivity (or specific conductivity) and K_{max} is the measured value that represents the potential maximum K. K values obtained after flushing the segment to remove native emboli are typically used for K_{max} (Sperry *et al.*, 1988). Most studies assume that observed K_{max} is equal to k_{sat}, the 'true' hydraulic conductivity at $P = 0$ (or the 'saturated' hydraulic conductivity). Because we cannot measure PLC or k_{sat} exactly, and K_{max} is rarely equal to k_{sat}, we choose to fit conductivity (not PLC) curves to measured K values. For clarity, we use upper-case K when referring to

observations and lower-case k for the 'expected' hydraulic conductivity that is described by a particular vulnerability curve. The relationship between expected percentage loss of conductivity (*plc*) and hydraulic conductivity (k) is given by:

$$plc = \frac{k_{sat} - k}{k_{sat}} \times 100 \quad \text{and} \quad k = k_{sat}\left(1 - \frac{plc}{100}\right) \qquad \text{Eqn 1}$$

Thus, a model for k yields an explicit model for *plc* and vice versa.

In this study, we re-evaluate two vulnerability curve models: the exponential-sigmoid (Pammenter & Vander Willigen, 1998) and the Weibull (Rawlings & Cure, 1985; Neufeld *et al.*, 1992). The equations for these vulnerability models are summarized in Table 1. Pammenter & Vander Willigen (1998) promote the exponential-sigmoid model because the parameters have biological meaning. However, we show that both models can be reparameterized in terms of P_X and S_X, where X is an arbitrary percentage loss that is specified in the model-fitting procedure. This parameterization allows one to choose specific values of X that are of interest and to directly compare parameter estimates and model fits between different vulnerability models. There are several steps involved in reparameterizing the models (Supporting Information, Methods S1), yielding equations for *plc* and k as functions of P_X, S_X, and k_{sat}. We give the reparameterized k functions (Table 1); the reparameterized *plc* functions are derived using Eqn 1 and are given in Methods S1.

Table 2 Geographic, climate, and soil data for the two study sites from which *Juniperus scopulorum* (Rocky Mountain juniper) populations were sampled

	Tonto NF	Fidalgo Island
Latitude	34°13′N	48°22′N
Longitude	111°15′W	122°31′W
Elevation (m)	1410	15
Mean annual precipitation (mm)	560.6	663.4
Mean June-September precipitation (mm)	192.3	118.4
Mean annual maximum temperature (°C)	22.9	14.8
Mean July maximum temperature (°C)	33.8	22.2
Soil type	Typic Haplustalf, loamy-skeletal, mixed, mesic	Lithic Haploxeroll, rock outcrop complex
Soil depth	'deep'	'shallow'

Climate data were obtained for the nearest weather stations (Payson, AZ, for Tonto NF and Anacortes, WA, for Fidalgo Island). Mean precipitation and temperature indices are for 1971–2000. Soil information was obtained from the USDA Natural Resources Conservation Service Soil Survey Report of Skagit County Area, Washington (1989) for Fidalgo Island, and from the USDA Forest Service, Southwestern Region, Terrestrial Ecosystems Survey Report for Tonto National Forest Northern Portion (1985).

The exponential-sigmoid model (Pammenter & Vander Willigen, 1998) is probably the most popular vulnerability curve and has been fitted to PLC data for a variety of woody species (Piñol & Sala, 2000; Martínez-Vilalta *et al.*, 2002; Choat *et al.*, 2003; McElrone *et al.*, 2004; Maherali *et al.*, 2006; Cochard *et al.*, 2008; Willson *et al.*, 2008). The reparameterized k function for the exponential-sigmoid is given by Eqn 1.3 (in Table 1) and is also described in Methods S1. If we assume that hydraulic conductivity at $P = 0$ MPa is given by $k(P = 0) = k_{sat}$, then according to Eqn 1, $plc(P = 0)$ must equal 0%. However, a potential problem of using the exponential-sigmoid model is that $plc(P = 0) \neq 0\%$ and $k(P = 0) \neq k_{sat}$. Moreover, plc and k are undefined for $X = 0\%$ and $X = 100\%$. Notice that, for the exponential-sigmoid, if $X = 50\%$ then the original parameters are given by $a = -(S_{50})/25$ and $b = P_{50}$ (Methods S1).

The Weibull function is also a commonly employed vulnerability model (Neufeld *et al.*, 1992; Sperry & Saliendra, 1994; Kavanagh *et al.*, 1999; Kolb & Sperry, 1999; Stiller & Sperry, 2002; Li *et al.*, 2008), and it has the longest history of use with respect to PLC analysis. Like the exponential-sigmoid model, the reparameterized k (Eqn 1.4, Table 1) is not defined for $X = 100\%$, but is defined for $X = 0\%$. An attractive feature of the Weibull model is that it does, in fact, satisfy $plc(P = 0) = 0\%$ and $k(P = 0) = k_{sat}$.

The reparameterized equations for k (and plc) for the exponential-sigmoid and Weibull models are highly nonlinear, both with respect to the independent variable P, and, more importantly, with respect to the parameters P_X, S_X, and k_{sat}. The original models are also nonlinear functions of P and their associated parameters. Thus, statistical methods that can accommodate this nonlinearity are required for fitting the reparameterized models to hydraulic conductivity data. Furthermore, each study may lead to a different way of specifying the statistical model depending on experimental design and sampling methods. The statistical model should be appropriately defined to capture the stochastic nature of the

data and cavitation process, to explicitly account for multiple sources of uncertainty, and to incorporate the expected, nonlinear conductivity curve. We first present the field study and sampling design for our *J. scopulorum* dataset, then we construct the statistical model.

Field study and conductivity data

Samples were collected from two *J. scopulorum* populations near the northern (Washington Park, Fidalgo Island, Skagit Co., WA, USA) and southern (Tonto National Forest, Gila Co., near Payson, AZ, USA) extremes of the species' distribution. We note, however, that since the collection of these samples, the Fidalgo population has been reclassified as a new, closely related species, *J. maritima* (Adams, 2007). For the purpose of this study, however, we will refer to both populations as *J. scopulorum*. Table 2 provides summaries of the study site locations, including climate and soil characteristics. To increase our chances of obtaining samples with relatively few native emboli, we obtained samples in the morning and during relatively wet periods of the growing season (May 2002, Fidalgo; September 2003, Payson). One branch and one root segment were collected from each of six mature *J. scopulorum* trees per site. Thus, a total of 12 trees were sampled (six trees × two sites), yielding 12 branch segments (one per tree) and 12 root segments (one per tree). Branches 0.5–0.7 m in length were clipped from the bottom third of the canopy, and roots 0.3–0.4 m in length were excavated from 15 to 30 cm soil depth.

Field preparation of samples and laboratory measurements of hydraulic conductivity followed the methods described in Willson *et al.* (2008). Briefly, the centrifugal force method (Pockman *et al.*, 1995; Alder *et al.*, 1997) was used to subject segments to progressively more negative water potentials. The eight pressures applied to the Fidalgo segments were 1, 2, 3, 4, 5.5, 7, 8.5, and 10 MPa; and the seven applied to the Payson segments were 2, 4, 5.5, 7, 8.5, 10, and 12 MPa. All

segments were initially flushed with water to remove native embolisms. Although it is common practice to assume that the water potential following flushing is equal to 0 MPa, we recognize that there is uncertainty associated with this assumption and treat the post-flushing water potential as unknown. Following each water potential treatment, hydraulic conductivity (K_H; kg m MPa^{-1} s^{-1}) was measured on each segment as described in Sperry *et al.* (1988) and Willson *et al.* (2008). To account for the effect of different cross-sectional sapwood areas (A), we determined A for each segment and calculated specific conductivity ($K_S = K_H/A$; kg m^{-1} MPa^{-1} s^{-1}). Both K_H and K_S varied by several orders of magnitude between segments; thus, for the statistical analysis, we found it convenient to work, instead, with relative conductivity (K). We computed K for each segment by dividing each of the segment's seven or eight K_H values by the K_H value measured directly following flushing, and all K values associated with flushing were equal to one. Importantly, the use of K instead of K_H or K_S does not compromise the interpretation of the P_X and S_X parameters.

In short, we can view the sampling design in this study as analogous to a split-plot experimental design (Steel *et al.*, 1997; Kutner *et al.*, 2004) with repeated measures. Trees are 'whole-plot' units and segments are 'split-plot' units, with site being the whole-plot 'treatment' and organ type (root or branch) being the split-plot treatment. The repeated aspect arises from each segment being measured for conductivity at each of several water potential values.

Hierarchical statistical model

We present a hierarchical Bayesian (HB) model (Ogle & Barber, 2008) that accommodates: (i) the unknown water potentials associated with flushing; (ii) the split-plot sampling design; and (iii) the nonlinear 'process' models that describe vulnerability to cavitation. Although many aspects of the statistical model could be implemented in a classical nonlinear, mixed-effects modeling framework, the HB approach (Wikle, 2003; Clark, 2005) has proved particularly useful for dealing with complicated models such as the ones presented herein. The HB model is composed of three stages: the data model (or likelihood) (stage 1), the process model (stage 2), and the parameter (or prior) model (stage 3) (Wikle, 2003; Clark, 2005; Ogle & Barber, 2008). Together, these stages give the joint posterior distribution of unknown parameters such as variance terms, the initial (flushing) water potentials, and P_X, S_X, and k_{sat} values associated with the segment, tree, site, and organ type levels. Moreover, it is straightforward to estimate differences in, for example, P_{50} between sites and organ types based on the posterior distribution of P_{50}. We describe each HB stage in the context of the *J. scopulorum* dataset.

Stage 1: the data model   We assume that observed relative conductivity (K) can be described by a normal distribution

with a mean given by the 'true' (or latent) relative conductivity (μ). For measurement m made on segment i of organ type t and from tree j in site s, the associated likelihood component for K is given by:

$$K_{\{m,i,j,t,s\}} \sim \text{Normal}\left(\mu_{\{m,i,j,t,s\}}, \sigma_K^2\right) \qquad \text{Eqn 2}$$

Here, the variance σ_K^2 represents observation error variability, and we assume that, conditional on the latent value (μ), the observation errors are independent.

Denote $P_{\{m,i,j,t,s\}}$ as the pressure, or positive-valued water potential, associated with each observed relative conductivity value in Eqn 2. We observed P for $m > 1$, but we do not have data on P for $m = 1$ as this represents the water potential after flushing. We assume that the segment-level unobserved flushing pressures are equal to a latent pressure that depends on organ type such that $P_{\{1,i,j,t,s\}} = P_{o\{t\}}$. Thus, P_o is an unknown parameter that we estimate.

Stage 2: the process model   Stage 2 specifies the process model for μ, and it incorporates a deterministic process mean model and stochastic process error. The process mean is defined by the expected vulnerability curve, and the process error describes discrepancies between the mean and latent relative conductivity:

$$\mu_{\{m,i,j,t,s\}} = k\left(P_{X\{i,j,t,s\}}, S_{X\{i,j,t,s\}}, k_{sat\{i,j,t,s\}} \mid P_{o\{t\}}, P_{\{m\neq1,i,j,t,s\}}\right) + \varepsilon_{\{m,i,j,t,s\}}$$

$$\text{Eqn 3}$$

The process mean $k(P_X, S_X, k_{sat} \mid P_o, P)$ is given by the reparameterized exponential-sigmoid or Weibull curve in Eqns 1.3 or 1.4, respectively (Table 1). The conditional notation in Eqn 3 indicates that k is a function of the stochastically specified parameters P_X, S_X, and k_{sat}, the stochastic initial P_o, and the fixed covariate P (the applied positive-valued pressure). Complex error structure is more commonly specified in the process error than observation error, and we explore two alternative formulations for the process errors, $\varepsilon_{\{m,i,j,t,s\}}$.

The simplest model assumes no process error so that all $\varepsilon_{\{m,i,j,t,s\}}$ terms are zero, and μ is exactly equal to $k(P_X, S_X, k_{sat} \mid P_o, P)$. The second model considers the stochastic nature of embolism. At xylem water potentials that cause intermediate amounts of cavitation, and in the absence of freezing stress, conduits of different sizes are assumed to cavitate with some probability that depends on the water potential, but this probability is expected to be independent of conduit size. At intermediate values of water stress, the size and number of conduits that do cavitate are a stochastic function of xylem water potential and the current state of filled and embolized conduits; this uncertainty in the cavitation process is revealed as a relatively wide range of probable conductivities compared with the extremes. That is, at extreme water stresses, we may

expect nearly complete cavitation of all conduits (high P) or nearly no cavitation of conduits ($P \cong 0$). In either case, we expect a relatively small potential range of conductivity values. Hence, we assume that the process error is a function of the expected *plc* such that:

$$\epsilon_{\{m,i,j,t,s\}} \sim \text{Normal}\left(0, \sigma^2_{P\{m,i,j,t,s\}}\right) \qquad \text{Eqn 4}$$

and

$$\sigma^2_{P\{m,i,j,t,s\}} = \eta^2_P \left(\frac{plc_{\{m,i,j,t,s\}}\left(100 - plc_{\{m,i,j,t,s\}}\right)}{2500} \right) \qquad \text{Eqn 5}$$

The process error is zero when all conduits are water-filled and functional (*plc* = 0%) or when all conduits have cavitated (*plc* = 100%), and all uncertainty in the conductivity data is attributed to observation error in this case. A maximum variance of $\sigma^2_{P\{m,i,j,t,s\}} = \eta^2_P$ occurs when *plc* = 50%. Note that *plc* in Eqn 5 is given by Eqn 1 with k as in Eqns 1.3 or 1.4 (Table 1).

Stage 3: the parameter model The primary quantities of interest are the conductivity process parameters (P_X, S_X, k_{sat}), and we assume that each segment has its own set of parameters. We model each hierarchically such that our model for each parameter is exactly analogous to that of a split-plot design whereby we account for segment effects nested within a tree effect, along with the effects for organ type, site, and their interaction. The sampling design determines how we model each parameter, and the parameter model can be modified to accommodated different designs or hierarchical structures. For our study, at the segment level, we have:

$$P_{X\{i,j,t,s\}} \sim \text{Normal}\left(\bar{P}_{X\{j,t,s\}}, \upsilon^2_{P_X}\right)$$
$$S_{X\{i,j,t,s\}} \sim \text{Normal}\left(\bar{S}_{X\{j,t,s\}}, \upsilon^2_{S_X}\right) \qquad \text{Eqn 6}$$
$$k_{sat\{i,j,t,s\}} \sim \text{Normal}\left(\bar{k}_{sat\{j,t,s\}}, \upsilon^2_{k_{sat}}\right)$$

where the variances $\upsilon^2_{P_X}$, $\upsilon^2_{S_X}$, and $\upsilon^2_{k_{sat}}$ describe between-segment variability. Negative values of P_X, S_X, and k_{sat} are biologically unrealistic, and thus the normal distributions in Eqn 6 are truncated at zero to ensure positive values for these parameters.

We use standard effects coding to model the means in Eqn 6, decomposing $\bar{P}_X$, $\bar{S}_X$, and $\bar{k}_{sat}$ into an organ type effect (α), a site effect (β), an organ type × site interaction effect ($\alpha\beta$), and a random tree effect (δ). The models for $\bar{P}_X$, $\bar{S}_X$, and $\bar{k}_{sat}$ are given by:

$$\bar{P}_{X\{j,t,s\}} = \alpha_{P_X\{t\}} + \alpha\beta_{P_X\{t,s\}} + \delta_{P_X\{j,s\}}$$
$$\bar{S}_{X\{j,t,s\}} = \alpha_{S_X\{t\}} + \alpha\beta_{S_X\{t,s\}} + \delta_{S_X\{j,s\}} \qquad \text{Eqn 7}$$
$$\bar{k}_{sat\{j,t,s\}} = \alpha_{k_{sat}\{t\}} + \alpha\beta_{k_{sat}\{t,s\}} + \delta_{k_{sat}\{j,s\}}$$

and

$$\delta_{P_X\{j,s\}} \sim \text{Normal}\left(\mu_{P_X} + \beta_{P_X\{s\}}, \tau^2_{P_X}\right)$$
$$\delta_{S_X\{j,s\}} \sim \text{Normal}\left(\mu_{S_X} + \beta_{S_X\{s\}}, \tau^2_{S_X}\right) \qquad \text{Eqn 8}$$
$$\delta_{k_{sat}\{j,s\}} \sim \text{Normal}\left(\mu_{k_{sat}} + \beta_{k_{sat}\{s\}}, \tau^2_{k_{sat}}\right)$$

where the parameters $\tau^2_{P_X}$, $\tau^2_{S_X}$, and $\tau^2_{k_{sat}}$ are variance components describing variability among trees after accounting for site. Although random effects are usually centered about zero, as with split-plot effects or whole-plot effects in a typical split-plot model, we choose the term 'tree effect' for δ, although it is centered on the sum of an overall effect (μ) plus a site effect (β). This is consistent with how we specify the model in WinBUGS (see section on Model implementation, below). Thus, the Eqns 6–8 are equivalent to the typical split-plot specification for each parameter. Also of interest is the expected value (mean) for a particular segment's process parameter Y, which we denote as $\hat{Y}$ and is given by:

$$\hat{Y}_{\{t,s\}} = E\left(Y_{\{i,j,t,s\}}\right) = \mu_Y + \alpha_{Y\{t\}} + \beta_{Y\{s\}} + \alpha\beta_{Y\{t,s\}} \qquad \text{Eqn 9}$$

where Y is P_X, S_X, or k_{sat} in Eqn 6, and $\hat{Y}_{\{t,s\}}$ is $\hat{P}_{X\{t,s\}}$, $\hat{S}_{X\{t,s\}}$, or $\hat{k}_{sat\{t,s\}}$, which can also be thought of as the fixed-effects cell means for the four combinations of organ type (t) and site (s). It is straightforward to compute contrasts of interest. For example, if one is interested in making inferences about the difference in P_X between stems ($t = 1$) and roots ($t = 2$) at Fidalgo ($s = 1$), this is computed as $\hat{P}_{X\{1,1\}} - \hat{P}_{X\{2,1\}} = (\alpha_{P_X\{1\}} + \beta_{P_X\{1,1\}}) - (\alpha_{P_X\{2\}} + \beta_{P_X\{2,1\}})$. One could also compute an effect size as, for example, $\hat{P}_{X\{1,1\}}/\hat{P}_{X\{2,1\}}$. Importantly, the HB method gives the posterior distributions for such contrasts and effects sizes, but we focus on contrasts in this study.

Finally, we assigned relatively noninformative or diffuse prior distributions to all remaining parameters, including all fixed effects, the organ type initial pressures, and all variance terms. We used diffuse normal distributions with mean zero and large variances (set to 2000) for the μ, α, β, and $\alpha\beta$ parameters, and we implemented 'sum-to-zero' constraints for the α, β, and $\alpha\beta$ parameters as is typically implied by this (factor) effects coding approach (Kutner *et al.*, 2004). We used semi-informative priors for the initial pressures by assigning a uniform distribution between 0 and 2 MPa to P_o because we expect the initial (positive-valued) water potential to be between zero and the first pressure applied via the centrifuge method (*c.* 2 MPa). Following Gelman (2006), we specified uniform, $U(0, A)$, priors for all standard deviations (i.e. σ_K, η_P, and the υ and τ values), where a value of A was chosen separately for each parameter.

Model implementation

The product of a Bayesian analysis is a joint posterior distribution of the unknown parameters given the data

Fig. 1 Observed vs predicted relative conductivity for the exponential-sigmoid (Exp-sig) model with process error (a) and the Weibull model with process error (b). Each point is the pair of observed relative conductivity (K) and the associated posterior mean for the replicated relative conductivity (K_{rep}). The diagonal lines are the least-squares regression fits (equation and R^2 provided), which are indistinguishable from the 1:1 line. The upper and lower curved lines represent the 95% prediction interval. Similar results were obtained for the models that did not incorporate process error.
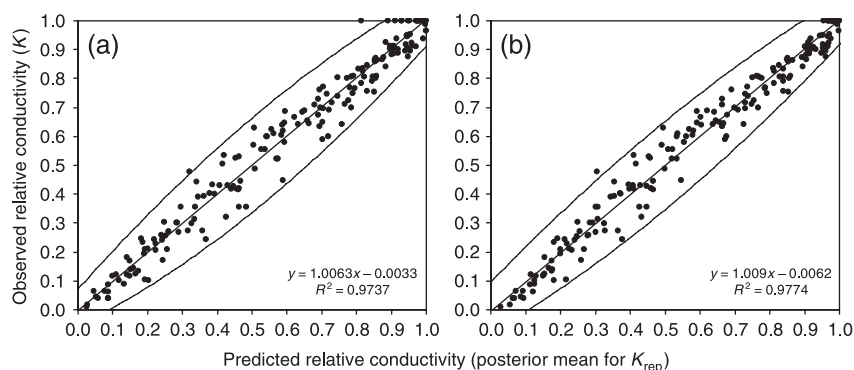
(Gelman *et al.*, 2004). Usually Markov chain Monte Carlo (MCMC) algorithms (Robert & Casella, 1999) are implemented to sample from the joint posterior, and from these samples one can calculate measures of centrality (e.g. mean, median, mode), spread (e.g. credible intervals, which are similar to confidence intervals), and correlations between parameters. We implemented the HB models in WinBUGS (Lunn *et al.*, 2000). We ran at least three parallel MCMC chains, evaluated the chains for convergence, and thinned chains when appropriate to reduce within-chain autocorrelation, thereby producing a sample of 4000 nearly independent draws from the posterior. In all cases, we set $X = 50\%$ and estimated P_{50} and S_{50}; however, it is easy to modify the WinBUGS code to obtain posterior distributions of P_X and S_X for different values of X. We illustrate this by computing posterior statistics for $X = 25$, 75, 90, and 99% for the Weibull model with process errors as given by Eqns 4 and 5.

Results

Model behavior and model comparison

We evaluated four different models defined by combinations of two process means (exponential sigmoid vs Weibull) and two process error assumptions (no process error vs stochastic process error). The MCMC chains for all parameters associated with both Weibull models exhibited good mixing (i.e. explored the posterior parameter space well with relatively little within-chain autocorrelation). While the chains for most parameters were well behaved in the exponential-sigmoid models, those related to the k_{sat} parameters were less well behaved, potentially because the exponential-sigmoid function is not anchored at $k = k_{sat}$ when $P = 0$ MPa. In contrast, k_{sat} is exactly the expected maximum relative conductivity (at $P = 0$) in the Weibull models, and thus measurements near $P = 0$ help to constrain the value of k_{sat} in this model wherein chains were better behaved. We first compare the performance of the four different models before presenting estimates for k_{sat} and important drought-tolerance parameters.

We used the deviance information criterion (DIC) described by Spiegelhalter *et al.* (2002) to compare the models. DIC

has two components: one describes model goodness-of-fit and the other penalizes for the number of 'effective' parameters. A difference in DIC values of five or more units indicates strong support for the model with the lowest DIC (Spiegelhalter *et al.*, 2002). The Weibull model with process error had the smallest DIC (−566.8), the exponential-sigmoid without process error had the largest DIC (−536.7), and the other two models had similar DIC values (*c.* −555), indicating exceptionally strong support for the Weibull model with process error. The models differed little in their effective number of parameters, which ranged from 49 (exponential-sigmoid without process error) to 53 (Weibull with process error), and thus differences in DIC are primarily the result of differences in model goodness-of-fit. If we only consider the Weibull models, the posterior mean for the observation standard deviation, σ_K, was 0.0550 for the model without process error; the model with process error yielded posterior means for the observation and process standard deviations, σ_K and η_P, of 0.0362 and 0.0570, respectively. Thus, the variability attributed to stochastic embolisms can be almost two times greater than the variability introduced by the observation (or measurement) process. Overall, the DIC values and estimates of the different variance components suggest that the Weibull model is superior to the exponential-sigmoid model, and the incorporation of stochastic process errors greatly improves model fit. The latter point is particularly important because other approaches do not consider such process errors, but this study indicates that the nonconstant variability introduced by stochastic embolisms is an important source of uncertainty.

These results are further supported by evaluations of model goodness-of-fit that compare observed vs predicted relative conductivity. We define the predicted values as the posterior mean for each 'replicated' relative conductivity observation, $K_{rep\{m,i,j,t,s\}}$, associated each observed value, $K_{\{m,i,j,t,s\}}$ (Gelman *et al.*, 2004). That is, K_{rep} values were generated from the same sampling distribution in Eqn 2, yielding the posterior predictive distribution for each K_{rep}. All four models generally resulted in similar patterns of observed vs predicted, wherein the points fell around the 1:1 line with R^2 values exceeding 0.97 (see Fig. 1 for the two models that included process error). Although the observed vs predicted plots look fairly similar
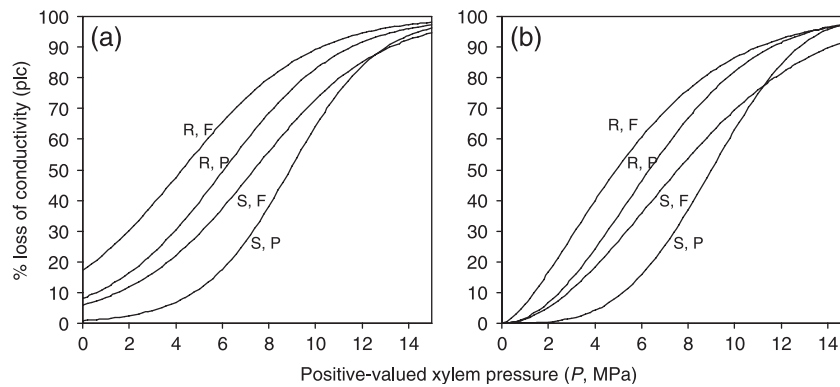
Fig. 2 Predicted 'expected' curves for percentage loss of hydraulic conductivity (*plc*) based on parameter estimates obtained from the exponential-sigmoid model with process error (a) and the Weibull model with process error (b). The *plc* curves were obtained by the following procedure. Posterior means for the cell means for P_{50} and S_{50} (see Fig. 4) were plugged into the equations for expected relative conductivity (*k*) (i.e. Eqn 1.3 for the exponential-sigmoid and Eqn 1.4 for the Weibull model; Table 1), and the equations were evaluated for different values of *P*. Then *plc* was computed according to Eqn 1. The four *plc* curves in each panel represent the predicted *plc* curves for roots from *Juniperus scopulorum* (Rocky Mountain juniper) from Fidalgo (R, F), roots from Payson (R, P), stems from Fidalgo (S, F), and stems from Payson (S, P).

between the exponential-sigmoid and Weibull models, one obvious difference is that the exponential-sigmoid has a difficult time fitting observed values of $K = 1.0$, whereas these values are 'pulled' more towards the 1:1 line by the Weibull model (Fig. 1). It is also fairly clear that the variability in the observed values tends to be smaller near the extremes (i.e. near $K = 0$ and $K = 1$), indicating that the stochastic process error model in Eqn 5 is necessary to describe this nonconstant variance accurately.

Despite similar observed vs predicted plots (Fig. 1), a comparison of the predicted vulnerability curves given by the exponential-sigmoid and the Weibull models clearly indicates that the Weibull model is more biologically consistent. Regardless of the process error model, the Weibull model gives $plc(P = 0) = 0\%$ exactly (see Fig. 2b for the Weibull model with process error). Conversely, the exponential-sigmoid predicts relatively high percentage loss of conductivity (*plc*) at $P = 0$ MPa (Fig. 2a). For example, the posterior mean and 95% central credible interval (CI) for $plc(P = 0)$ for roots from the Payson site are 18.0% and [7.2%, 32.0%] for the exponential-sigmoid model with process error (Fig. 2a). The nonzero *plc*-intercept for the exponential-sigmoid model is a direct artifact of its functional form such that for $X = 50\%$,

$$plc(P = 0) = 100 \left(1 + \exp\left(\frac{P_{50} S_{50}}{25} \right) \right)^{-1}$$

Thus, based on this model, *plc* curves for plants or organ types that are highly vulnerable to cavitation will necessarily have a high *plc*-intercept regardless of whether or not this is biologically realistic.

In summary, these results yield two important suggestions for the analysis of data on vulnerability to cavitation. First, the nonconstant variance associated with stochastic embolisms is an important source of uncertainty that should be included in such analyses. Second, the Weibull model is superior to the exponential-sigmoid model and is thus the preferred 'expected process' model for such analyses.

Parameter estimates for *J. scopulorum*

Given the preceding discussion, from this point forward, we focus on models that incorporate stochastic process errors. The exponential-sigmoid model resulted in less realistic and less accurate estimates for the segment-level k_{sat} (Eqn 6) estimates compared with the Weibull model. For the exponential-sigmoid model, the posterior means for the segment-level k_{sat} values ranged from 1.00 to 1.19, and the 95% CI widths ranged from 0.06 to 0.32, whereas, for the Wiebull model, the posterior means and 95% CI widths ranged from 0.97 to 1.01 and 0.07 to 0.09, respectively. The high uncertainty in these segment-level values associated with the exponential-sigmoid vs Weibull model is also reflected in the cell means estimates for $\hat{k}_{sat}$ (Fig. 3), Eqn 9. Both exponential-sigmoid models yielded higher-than-expected values for $\hat{k}_{sat}$ (i.e. typically greater than 1), whereas both Weibull models yielded values that were generally centered around one with high precision (narrow CIs) (e.g. Fig. 3). It is worth comparing the $\hat{k}_{sat}$ estimates (Fig. 3) with the predicted *plc* curves (Fig. 2). The *plc* curve for stems from Payson given by the exponential-sigmoid goes through approx. 0% at $P = 0$ MPa (Fig. 2a), and is thus is a biologically realistic curve, and the $\hat{k}_{sat}$ estimate corresponding to this curve is also realistic (near 1.0) and well estimated (narrow CI) (Fig. 3). The other three *plc* curves given by the exponential-sigmoid have relatively high values for $plc(P = 0)$, accompanied by high values for $\hat{k}_{sat}$ that are also highly uncertain. Thus, the exponential-sigmoid has difficulties producing both realistic vulnerability curves and estimates of maximum hydraulic conductivity.
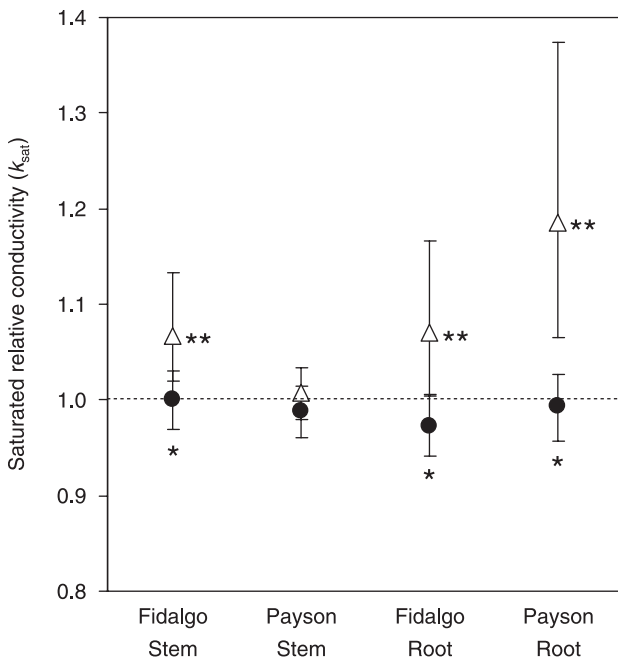
Fig. 3 Posterior means and 95% credible intervals (CIs) for the cell means for saturated (or maximum) relative hydraulic conductivity, $\hat{k}_{sat}$, Eqn 9, based on the Weibull (circles) and exponential-sigmoid (triangles) models with process error. For comparisons between models within a site and organ type, $\hat{k}_{sat}$ values are significantly different between models if the posterior mean given by one model is not contained in the other model's 95% CI, as indicated by an *. Individual $\hat{k}_{sat}$ values are considered different from 1.0 if their 95% CIs do not contain 1.0; $\hat{k}_{sat}$ values that differ from 1.0 are indicated by ** next the corresponding model's symbol.

Comparing parameter estimates between the models, three of the four $\hat{k}_{sat}$ estimates were significantly different between the two models. The $\hat{k}_{sat}$ value for stems from Payson was the only one that was similar between the models (Fig. 3). While the exponential-sigmoid generally produced $\hat{k}_{sat}$ estimates

that were significantly greater than 1 (Fig. 3), the $\hat{k}_{sat}$ estimates provided by the Weibull model did not differ from 1 (Fig. 3). Since the Weibull model yields biologically realistic vulnerability curves, this suggests that for this species (*J. scopulorum*), conductivity measurements following flushing closely approximate maximum conductivity. Unlike $\hat{k}_{sat}$, the important parameters describing drought-tolerance characteristics – the pressure resulting in $X = 50\%$ loss of hydraulic conductivity, $\hat{P}_{50}$, and the sensitivity of *plc* to changes in pressure at $P = \hat{P}_{50}$, $\hat{S}_{50}$ – did not differ significantly between the two models, in terms of both their posterior means and the estimates of uncertainty (i.e. CI widths). However, given that the Weibull is preferred over the exponential-sigmoid, we focus on the Weibull model with stochastic process errors from this point forward.

The posterior estimates for drought-tolerance parameters for *J. scopulorum* are shown in Fig. 4 for the Weibull model with process error. At the Fidalgo site, stems and roots do not differ significantly in their susceptibility to cavitation, such that the posterior means for $\hat{P}_{50}$ are 7.6 MPa for stems and 6.3 MPa for roots (Fig. 4a), and the 95% CI for the contrast $\hat{P}_{X\{1,1\}} - \hat{P}_{X\{2,1\}}$ contained zero: [−3.62, 1.16]. Conversely, at the Payson site, roots are significantly more vulnerable to cavitation than stems, such that the posterior means for the $\hat{P}_{50}$ of roots and shoots were 4.9 and 9.0 MPa, respectively, (Fig. 4a), and the 95% CI for the associated contrast did not contain zero: [−6.48, −1.68]. Based on the estimates for $\hat{P}_{50}$, susceptibility to cavitation does not differ between *J. scopulorum* growing at the northern (Fidalgo) and southern (Payson) sites (Fig. 4a). For example, the site and site × organ type interaction effects did not differ from zero; that is, the 95% CIs for α_{P_X} and $\alpha\beta_{P_X}$ (Eqn 7) were [−1.03, 1.04] and [−1.54, 0.12], respectively.

Sensitivity to changes in water potential at the 50% loss point also did not differ between stems and roots at Fidalgo (Fig. 4b); for example, the 95% CI for the contrast
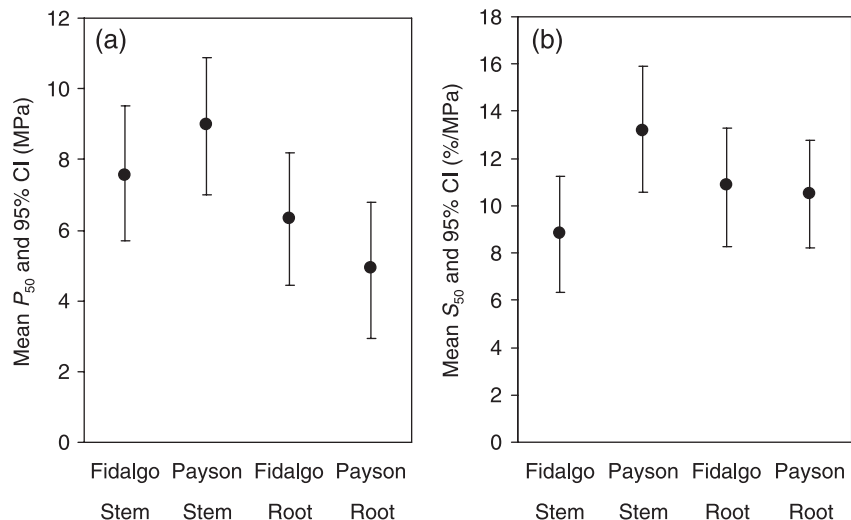
Fig. 4 Posterior means and 95% credible intervals (CIs) for the cell means for P_{50} and S_{50} obtained from the Weibull model with process error. Estimates are given for each organ type (*t*) and site (*s*) for the (positive-valued) water potential that results in 50% loss of hydraulic conductivity (i.e. $\hat{P}_{50\{t,s\}}$ as defined in Eqn 9) (a), and for the sensitivity of percentage loss of hydraulic conductivity at $P = \hat{P}_{50\{t,s\}}$ (i.e. $\hat{S}_{50\{t,s\}}$ as defined in Eqn 9) (b).

$\hat{S}_{X\{1,1\}} - \hat{S}_{X\{2,1\}}$ contained zero: [–0.96, 4.91]. Although the marginal means for $\hat{S}_{50}$ in Fig. 4b suggest that *J. scopulorum* stems from Payson were more sensitive (higher $\hat{S}_{50}$) to changes in water potentials than roots (Fig. 4b), the 95% CI for the associated contrast contained zero: [–5.6, 0.31], indicating that $\hat{S}_{50}$ also does not differ significantly between stems and roots in this site. Although $\hat{S}_{50}$ did not differ between roots in the two different sites, there is evidence that stems from Payson trees are more sensitive to changes in xylem water potential than stems from Fidalgo (Fig. 4b), and the 95% CI for the contrast $\hat{S}_{X\{2,1\}} - \hat{S}_{X\{2,2\}}$ did not contain zero: [–7.91, –0.81]. Moreover, although the site effect for the sensitivity parameter, α_{S_X}, did not differ from zero (i.e. the 95% CI was [–2.45, 0.41]), there was a significant site × organ type interaction such that the 95% CI for $\alpha\beta_{S_X}$ was [–2.18, –0.09]. Overall, stems from Fidalgo were least sensitive to changes in water potential, whereas stems from Payson were most sensitive to changes in water potential despite having the largest $\hat{P}_{50}$ value (i.e. least susceptible to drought-induced cavitation) (see Fig. 4b).

Discussion

Analysis of hydraulic conductivity data

Significant advancements have been made with respect to experimental methods for measuring vulnerability to cavitation (Brodribb & Holbrook, 2003; Kikuta *et al.*, 2003; Mayr & Cochard, 2003; Sperry *et al.*, 2003; Li *et al.*, 2008), but statistical methods for analyzing such data have lagged behind. This study aligns the statistical and experimental methodologies. First, we demonstrated that two common vulnerability curves can be reparameterized in terms of meaningful drought-tolerance parameters. Then we illustrated how these nonlinear models can be fitted to data on (relative) hydraulic conductivity using hierarchical Bayesian statistical methods that: (i) accommodate the sampling design (such as the split-plot design in this study); (ii) explicitly incorporate different sources of variability (such as process error introduced by stochastic embolism events); and (iii) explicitly estimate uncertainty associate with important drought-tolerance parameters via the posterior distribution. We believe that our explicit accounting of important sources of variability results in more realistic characterizations of the uncertainty in our predictions of xylem vulnerability to cavitation.

One goal of this study is to thoroughly evaluate the usefulness of the most commonly used vulnerability curves. A primary reason for the popularity of the exponential-sigmoid model is that its (original) parameters are equal to, or proportional to, drought-tolerance parameters (Pammenter & Vander Willigen, 1998; Domec & Gartner, 2001). Now that we have shown that both models can be reparameterized in terms of P_X, S_X, and k_{sat}, there is no clear justification for choosing the exponential-sigmoid over the Weibull curve. In fact, we encountered several problems when fitting the exponential-sigmoid to conductivity data for *J. scopulorum*. For example, some of the MCMC parameter chains did not mix well, the k_{sat} parameters were estimated with relatively low precision and were generally greater than 1, and predicted *plc* exceeded zero at water potentials of approx. 0 MPa. The problem that $plc > 0$ at $P = 0$ MPa for the exponential-sigmoid is a direct property of the model and is not unique to this study. In fact, several previous studies also give estimated exponential-sigmoid curves with plc intercepts that are greater than zero (Pammenter & Vander Willigen, 1998; Martínez-Vilalta *et al.*, 2002; Oliveras *et al.*, 2003) and some appear unreasonably high (Choat *et al.*, 2003). Hence, we recommend the Weibull model over the exponential-sigmoid model because the MCMC chains were well behaved and it provides more biologically realistic vulnerability curves that are anchored at 0% loss at 0 MPa.

We also note that the hierarchical Bayesian approach described herein is preferred to other methods such as maximum likelihood (ML). For example, to test for treatment effects (e.g. via contrasts) and to construct confidence intervals for parameters based on ML results requires a series of asymptotic normality approximations (Seber & Wild, 1989; Pinheiro & Bates, 2000). Given that parameters may not be adequately described by a normal distribution and that experimental studies can only measure a finite number of subjects, such approximations have the potential to misrepresent the degree of uncertainty in the data and parameter estimates (Seber & Wild, 1989). Conversely, the Bayesian analysis does not rely on such approximations and is not constrained to normal distributions. The posterior distributions can take any form, and thus the Bayesian parameter estimates and intervals may more accurately portray uncertainty (Gelman *et al.*, 2004). Bayesian and ML interval estimates may be similar, however, if the posterior distributions for the parameters are approximately normal, which was generally the case in this study for most parameters. Although, the posteriors for $P_{o\{t\}}$ could not be described by normal densities, which is to be expected since these parameters are expected to be close to a lower bound of 0 MPa.

Inferences about vulnerability to cavitation

Another major advantage of the methods described here is that it is easy to compute estimates for other parameters of interest, such as P_Y and S_Y ($Y \neq X$). For example, P_Y and S_Y can be written as functions of P_X and S_X, and for the Weibull model P_Y is:

$$P_Y = P_X \left(\frac{\ln\left(1 - \frac{Y}{100}\right)}{\ln\left(1 - \frac{X}{100}\right)} \right)^{\frac{V}{P_X S_X}} \qquad \text{Eqn 10}$$
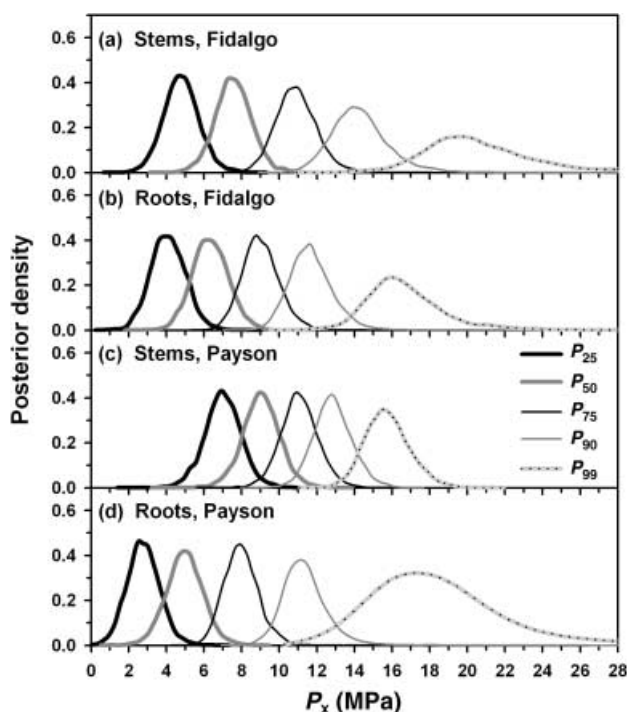
Fig. 5 Posterior distributions for the (positive-valued) water potentials that result in $X = 25, 50, 75, 90$, and 99% loss of hydraulic conductivity: P_{25}, P_{50}, P_{75}, P_{90}, and P_{99} for stems from *Juniperus scopulorum* (Rocky Mountain juniper) from Fidalgo (a), roots from Fidalgo (b), stems from Payson (c), and roots from Payson (d). The P_X estimates are based on the Weibull model with process error, and P_{25}, P_{75}, P_{90}, and P_{99} were calculated from the posterior samples for $\hat{P}_{50}$ and $\hat{S}_{50}$ using Eqn 10.

where V is defined in Table 1, Eqn 1.4 (Methods S1 gives solutions S_Y). Estimates of P_Y and S_Y are easily obtained by Bayesian methods. In practice, one would set $X = 50\%$ (or any arbitrary value between 0 and 100%) and fit the Weibull model in WinBUGS, which would produce a list of values for P_{50} and S_{50} (i.e. samples from the posterior). By applying Eqn 10 to the P_{50} and S_{50} posterior samples obtained from the MCMC simulation, one can obtain a posterior sample of P_Y (and S_Y). We illustrate this in Fig. 5 where we use the posterior samples of P_{50} and S_{50} to estimate posterior distributions of P_{25}, P_{75}, P_{90}, and P_{99} for *J. scopulorum*. Alternatively, one could re-run the Bayesian model for each Y, but this is not necessary, and each run could take several hours to converge.

A comparison of roots and stems from the two geographically distinct populations of *J. scopulorum* shows that differences in *plc* are greatest at high (less negative) water potentials, and these differences begin to fade as P or *plc* increases (e.g. compare differences in P_{25} between organ types and sites vs differences in P_{50}, P_{75}, P_{90}, and P_{99}, Fig. 5). If P_{25} (or some other P_Y for Y 'small') is used as an index of the onset of cavitation, then cavitation in stems from Payson is delayed, with respect to the xylem water potential required to induced 25% loss, compared with stems from Fidalgo and roots

from both locations. Since presumably higher water potentials are most frequently experienced in the field, and they must be experienced before more negative potentials develop, differences in *plc* within this range (e.g. < -5 MPa) may be particularly important to a plant's overall drought response. Thus, in addition to the standard use of P_{50}, the onset of cavitation (e.g. P_{25}, P_{10}) and/or the air-entry potential (Ψ_e or P_{12}) (Sparks & Black, 1999; Domec & Gartner, 2001) are key parameters that should be considered more frequently. If we also consider the other 'extreme' by evaluating cavitation under very negative water potentials, then this analysis suggests that *J. scopulorum* has the potential to maintain water transport capacity at water potentials of -10 to -16 MPa, the point at which almost 90% loss of hydraulic conductivity occurs (Fig. 5).

The drier, hotter climate in central Arizona as compared to the maritime climate of western Washington led us to hypothesize that differential vulnerability to cavitation may exist between the two *J. scopulorum* populations, and we anticipated that Payson trees would be more resistant than Fidalgo trees. This hypothesis, however, was not strongly supported by our data and analyses. Based on the P_X estimates, stems from Payson were slightly more resistant than roots and stems from Fidalgo at water potentials above c. -10 MPa (or $P < 10$), but roots from Payson were least drought-tolerant (Figs 4a, 5). Cavitation sensitivity (based on S_{50}) did not differ between sites for roots, but did differ for stems (Fig. 4b). In general, however, site-to-site variation in P_X and S_X was relatively small (Figs 4, 5), and lack of such intraspecific variation has also been shown for stems from other conifer species (Maherali & DeLucia, 2000; Martínez-Vilalta & Piñol, 2002). Greater differences were found between roots and stems within a site than between sites. At Payson, stems were significantly more resistant to cavitation than roots (Figs 4a, 5). This was expected, given that water potentials decrease from the soil to the leaves, emboli may be easier to repair in the roots as a result of positive root pressures (Tyree & Sperry, 1989), and the there is ample evidence that roots are more susceptible to cavitation than stems in several conifer species (Sperry & Ikeda, 1997; Linton *et al.*, 1998; Kavanagh *et al.*, 1999; Oliveras *et al.*, 2003; McElrone *et al.*, 2004).

An accurate estimate of maximum hydraulic (or specific) conductivity may also be desired because of its potential to regulate maximum photosynthetic capacity (Brodribb & Feild, 2000). Unlike previous analyses, our modeling framework recognizes that: (i) the xylem water potential associated with hydraulic conductivity measured after flushing is unknown; and (ii) saturated hydraulic conductivity is measured with error. The modeling framework herein acknowledges these two sources of uncertainty by estimating the initial water potential (P_o) and by fitting a vulnerability curve to conductivity data, not computed PLC values. For example, based on the Weibull model with process error, the

posterior means and 95% CIs for P_o for *J. scopulorum* stems and roots were 0.342 [0.013, 0.975] MPa and 0.065 [0.002, 0.233] MPa, respectively. These results indicate that the 'true' initial pressure is near zero, but not exactly equal to zero, as the posterior distribution was skewed towards 'larger' values.

Moreover, given the posterior estimates for the $\hat{k}_{sat}$ cell means (Fig. 3), we can compute estimates of the maximum specific conductivity (K_{Ssat}). For example, the $\hat{k}_{sat}$ posterior mean and 95% CI for stems from Payson were 0.99 and [0.96, 1.01] (Fig. 3), and the average measured initial K_S for these segments was 0.067 kg m^{-1} MPa^{-1} s^{-1}. Thus, the posterior mean and 95% CI for the predicted K_{Ssat} are $0.067 \times 0.99 = 0.066$ and [0.064, 0.067] kg m^{-1} MPa^{-1} s^{-1}. Applying the same calculations to stems from Fidalgo and roots from Payson and Fidalgo, the resulting posterior means and 95% CIs for K_{Ssat} are 0.499 [0.483, 0.514], 1.052 [1.015, 1.088], and 1.954 [1.887, 2.019] kg m^{-1} MPa^{-1} s^{-1}, respectively. Thus, roots and stems from the driest and southernmost extreme population of *J. scopulorum*'s distribution have significantly lower water transport capacity (i.e. lower K_{Ssat}) than those from the wetter, more northern population. Moreover, within both locations, water transport capacity of roots is an order of magnitude or more greater than that of stems in *J. scopulorum*, which is consistent with a variety of studies for woody plants (Kavanagh *et al.*, 1999; Martínez-Vilalta *et al.*, 2002; McElrone *et al.*, 2004). This exercise, however, illustrates that the explicit modeling of k_{sat} (and thus K_{Ssat}) means that one does not need to go to great lengths to remove all native emboli before measuring hydraulic conductivity. Instead, one should focus on making measurements over a range of water potentials that sufficiently span zero to 100% loss of conductivity.

In conclusion, although we illustrate the hierarchical Bayesian statistical methods using hydraulic conductivity data for *J. scopulorum* obtained under drought-induced cavitation experiments, the methods can be easily extended to analysis of vulnerability to cavitation during freeze–thaw cycles. Moreover, while the mathematical reparameterizations are specific to vulnerability curves, the statistical techniques may be appropriate for a wide variety of physiological data that are characterized by nonlinear response functions and mixed-effects error structures.

Acknowledgements

References

Adams RP. 2007. *Juniperus maritima*, the Seaside Juniper, a new species from Puget Sound, North America. *Phytologia* **89**: 263–283.

Alder NN, Pockman WT, Sperry JS, Nuismer S. 1997. Use of centrifugal force in the study of xylem cavitation. *Journal of Experimental Botany* **48**: 665–674.

Boyer JS. 1976. Photosynthesis at low water potentials. *Philosophical Transactions of the Royal Society of London. B.* **273**: 501–512.

Brodribb T, Hill RS. 1999. The importance of xylem constraints in the distribution of conifer species. *New Phytologist* **143**: 365–372.

Brodribb T, Holbrook NM. 2003. Stomatal closure during leaf dehydration, correlation with other leaf physiological traits. *Plant Physiology* **132**: 2166–2173.

Brodribb TJ, Feild TS. 2000. Stem hydraulic supply is linked to leaf photosynthetic capacity: evidence from new Caledonian and Tasmanian rainforests. *Plant, Cell & Environment* **23**: 1381–1388.

Choat B, Ball M, Luly J, Holtum J. 2003. Pit membrane porosity and water stress-induced cavitation in four co-existing dry rainforest tree species. *Plant Physiology* **131**: 41–48.

Clark JS. 2005. Why environmental scientists are becoming Bayesians. *Ecology Letters* **8**: 2–14.

Cochard H, Barigah ST, Kleinhentz M, Eshel A. 2008. Is xylem cavitation resistance a relevant criterion for screening drought resistance among *Prunus* species? *Journal of Plant Physiology* **165**: 976–982.

Cowan IR. 1982. Regulation of water use in relation to carbon gain in higher plants. In: Lange OL, Nobel PS, Osmond CB, Ziegler H, eds. *Physiological plant ecology Ii, water relations and carbon assimilation*. New York, NY, USA: Springer-Verlag, 589–613.

Domec JC, Gartner BL. 2001. Cavitation and water storage capacity in bole xylem segments of mature and young Douglas fir trees. *Trees-Structure and Function* **15**: 204–214.

Gelman A. 2006. Prior distributions for variance parameters in hierarchical models. *Bayesian Analysis* **1**: 515–533.

Gelman A, Carlin JB, Stern HS, Rubin DB. 2004. *Bayesian data analysis*. Boca Raton, FL, USA: Chapman & Hall/CRC.

Hacke UG, Sperry JS. 2001. Functional and ecological xylem anatomy. *Perspectives in Plant Ecology Evolution and Systematics* **4**: 97–115.

Hacke UG, Sperry JS, Pitterman J. 2000. Drought experience and cavitation resistance in six shrubs from the Great Basin, Utah. *Basic and Applied Ecology* **1**: 31–41.

Jacobsen AL, Pratt RB, Ewers FW, Davis SD. 2007. Cavitation resistance among 26 chaparral species of southern California. *Ecological Monographs* **77**: 99–115.

Kavanagh KL, Bond BJ, Aitken SN, Gartner BL, Knowe S. 1999. Shoot and root vulnerability to xylem cavitation in four populations of Douglas-fir seedlings. *Tree Physiology* **19**: 31–37.

Kikuta SB, Hietz P, Richter H. 2003. Vulnerability curves for conifer sapwood sections exposed over solutions with known water potentials. *Journal of Experimental Botany* **54**: 2149–2155.

Kolb KJ, Sperry JS. 1999. Differences in drought adaptation between subspecies of sagebrush (*Artemisia Tridentata*). *Ecology* **80**: 2373–2384.

Kutner MH, Nachtsheim CJ, Neter J, Li W. 2004. *Applied linear statistical models*. New York, NY, USA: McGraw-Hill.

Li YY, Sperry JS, Taneda H, Bush WE, Hacke UG. 2008. Evaluation of centrifugal methods for measuring xylem cavitation in conifers, diffuse- and ring-porous angiosperms. *New Phytologist* **177**: 558–568.

Linton MJ, Sperry JS, Williams DG. 1998. Limits to water transport in *Juniperus osteosperma* and *Pinus edulis*: implications for drought tolerance and regulation of transpiration. *Functional Ecology* **12**: 906–911.

Lunn DJ, Thomas A, Best N, Spiegelhalter D. 2000. Winbugs – a bayesian modelling framework: concepts, structure, and extensibility. *Statistics and Computing* **10**: 325–337.

Macinnis-Ng C, McClenahan K, Eamus D. 2004. Convergence in

hydraulic architecture, water relations and primary productivity amongst habitats and across seasons in Sydney. *Functional Plant Biology* **31**: 429–439.

Maherali H, DeLucia EH. 2000. Xylem conductivity and vulnerability to cavitation of ponderosa pine growing in contrasting climates. *Tree Physiology* **20**: 859–867.

Maherali H, Moura CF, Caldeira MC, Willson CJ, Jackson RB. 2006. Functional coordination between leaf gas exchange and vulnerability to xylem cavitation in temperate forest trees. *Plant, Cell & Environment* **29**: 571–583.

Martínez-Vilalta J, Piñol J. 2002. Drought-induced mortality and hydraulic architecture in pine populations of the NE Iberian Peninsula. *Forest Ecology and Management* **161**: 247–256.

Martínez-Vilalta J, Prat E, Oliveras I, Piñol J. 2002. Xylem hydraulic properties of roots and stems of nine Mediterranean woody species. *Oecologia* **133**: 19–29.

Mayr S, Cochard H. 2003. A new method for vulnerability analysis of small xylem areas reveals that compression wood of Norway spruce has lower hydraulic safety than opposite wood. *Plant, Cell & Environment* **26**: 1365–1371.

McElrone AJ, Pockman WT, Martínez-Vilalta J, Jackson RB. 2004. Variation in xylem structure and function in stems and roots of trees to 20 m depth. *New Phytologist* **163**: 507–517.

Mencuccini M, Comstock J. 1997. Vulnerability to cavitation in populations of two desert species, *Hymenoclea salsola* and *Ambrosia dumosa*, from different climatic regions. *Journal of Experimental Botany* **48**: 1323–1334.

Neufeld HS, Grantz DA, Meinzer FC, Goldstein G, Crisosto GM, Crisosto C. 1992. Genotypic variability in vulnerability of leaf xylem to cavitation in water-stressed and well-irrigated sugarcane. *Plant Physiology* **100**: 1020–1028.

Ogle K, Barber JJ. 2008. Bayesian data-model integration in plant physiological and ecosystem ecology. *Progress in Botany* **69**: 281–311.

Oliveras I, Martínez-Vilalta J, Jimenez-Ortiz T, Lledó MJ, Escarré A, Piñol J. 2003. Hydraulic properties of *Pinus halepensis*, *Pinus pinea* and *Tetraclinis articulata* in a dune ecosystem of Eastern Spain. *Plant Ecology* **169**: 131–141.

Pammenter NW, Vander Willigen C. 1998. A mathematical and statistical analysis of the curves illustrating vulnerability of xylem to cavitation. *Tree Physiology* **18**: 589–593.

Peek MS, Russek-Cohen E, Wait DA, Forseth IN. 2002. Physiological response curve analysis using nonlinear mixed models. *Oecologia* **132**: 175–180.

Pinheiro JC, Bates DM. 2000. *Mixed-effects models in S and S-plus*. New York, NY, USA: Springer-Verlag.

Piñol J, Sala A. 2000. Ecological implications of xylem cavitation for several Pinaceae in the Pacific Northern USA. *Functional Ecology* **14**: 538–545.

Pockman WT, Sperry JS. 2000. Vulnerability to xylem cavitation and the distribution of Sonoran Desert vegetation. *American Journal of Botany* **87**: 1287–1299.

Pockman WT, Sperry JS, O'Leary W. 1995. Sustained and Significant Negative Water Pressure in Xylem. *Nature* **378**: 715–716.

Potvin C, Lechowicz MJ, Tardif S. 1990. The statistical analysis of ecophysiological response curves obtained from experiments involving repeated measures. *Ecology* **71**: 1389–1400.

Rawlings JO, Cure WW. 1985. The weibull function as a dose-response model to describe ozone effects on crop yields. *Crop Science* **25**: 807–814.

Robert CP, Casella G. 1999. *Monte Carlo statistical methods*. New York, NY, USA: Springer-Verlag.

Seber GAF, Wild CJ. 1989. *Nonlinear regression*. New York, NY, USA: Wiley.

Sparks JP, Black RA. 1999. Regulation of water loss in populations of *Populus trichocarpa*: the role of stomatal control in preventing xylem cavitation. *Tree Physiology* **19**: 453–459.

Sperry JS. 1995. Limitations of stem water transport and their consequences. In: Gartner BL, ed. *Plant stems: physiology and functional morphology*. San Diego, CA, USA: Academic Press, 105–124.

Sperry JS. 2000. Hydraulic constraints on plant gas exchange. *Agricultural and Forest Meteorology* **104**: 13–23.

Sperry JS, Adler FR, Campbell GS, Comstock JP. 1998. Limitation of plant water use by rhizosphere and xylem conductance: results from a model. *Plant, Cell & Environment* **21**: 347–359.

Sperry JS, Donnelly JR, Tyree MT. 1988. A method for measuring hydraulic conductivity and embolism in xylem. *Plant, Cell & Environment* **11**: 35–40.

Sperry JS, Ikeda T. 1997. Xylem cavitation in roots and stems of Douglas-fir and white fir. *Tree Physiology* **17**: 275–280.

Sperry JS, Pockman WT. 1993. Limitation of transpiration by hydraulic conductance and xylem cavitation in *Betula occidentalis*. *Plant, Cell & Environment* **16**: 279–287.

Sperry JS, Saliendra NZ. 1994. Intra-plant and inter-plant variation in xylem cavitation in *Betula occidentalis*. *Plant, Cell & Environment* **17**: 1233–1241.

Sperry JS, Stiller V, Hacke UG. 2003. Xylem hydraulics and the soil-plant-atmosphere continuum: opportunities and unresolved issues. *Agronomy Journal* **95**: 1362–1370.

Sperry JS, Sullivan JEM. 1992. Xylem embolism in response to freeze-thaw cycles and water-stress in ring-porous, diffuse-porous, and conifer species. *Plant Physiology* **100**: 605–613.

Sperry JS, Tyree MT. 1990. Water-stress-induced xylem embolism in three species of conifers. *Plant, Cell & Environment* **13**: 427–436.

Spiegelhalter DJ, Best NG, Carlin BR, van der Linde A. 2002. Bayesian measures of model complexity and fit. *Journal of the Royal Statistical Society Series B-Statistical Methodology* **64**: 583–616.

Steel RGD, Torrie JH, Dickey DA. 1997. *Principles and procedures of statistics: a biometrical approach*. New York, NY, USA: McGraw-Hill.

Stiller V, Sperry JS. 2002. Cavitation fatigue and its reversal in sunflower (*Helianthus Annuus* L.). *Journal of Experimental Botany* **53**: 1155–1161.

Tyree MT, Ewers FW. 1991. The hydraulic architecture of trees and other woody plants. *New Phytologist* **119**: 345–360.

Tyree MT, Sperry JS. 1988. Do woody plants operate near the point of catastrophic xylem dysfunction caused by dynamic water-stress: answers from a model. *Plant Physiology* **88**: 574–580.

Tyree MT, Sperry JS. 1989. Vulnerability of xylem to cavitation and embolism. *Annual Review of Plant Physiology and Plant Molecular Biology* **40**: 19–38.

Wang J, Ives NE, Lechowicz MJ. 1992. The relation of foliar phenology to xylem embolism in trees. *Functional Ecology* **6**: 469–475.

Wikle CK. 2003. Hierarchical models in environmental science. *International Statistical Review* **71**: 181–199.

Willson CJ, Manos PS, Jackson RB. 2008. Hydraulic traits are influenced by phylogenetic history in the drought-resistant, invasive genus Juniperus (Cupressaceae). *American Journal of Botany* **95**: 299–314.

Zimmermann MH. 1983. *Xylem structure and the ascent of sap*. New York, NY, USA: Springer-Verlag.

Supporting Information

Additional supporting information may be found in the online version of this article.

Methods S1 Reparameterizing the vulnerability curve models.

Methods S2 WinBUGS code for the Weibull model with process error.

Please note: Wiley-Blackwell are not responsible for the content or functionality of any supporting information supplied by the authors. Any queries (other than missing material) should be directed to the *New Phytologist* Central Office.

About *New Phytologist*

- *New Phytologist* is owned by a non-profit-making **charitable trust** dedicated to the promotion of plant science, facilitating projects from symposia to open access for our Tansley reviews. Complete information is available at **www.newphytologist.org**.

- Regular papers, Letters, Research reviews, Rapid reports and both Modelling/Theory and Methods papers are encouraged. We are committed to rapid processing, from online submission through to publication 'as-ready' via *Early View* – our average submission to decision time is just 29 days. Online-only colour is **free**, and essential print colour costs will be met if necessary. We also provide 25 offprints as well as a PDF for each article.

- For online summaries and ToC alerts, go to the website and click on 'Journal online'. You can take out a **personal subscription** to the journal for a fraction of the institutional price. Rates start at £139 in Europe/$259 in the USA & Canada for the online edition (click on 'Subscribe' at the website).

- If you have any questions, do get in touch with Central Office (**newphytol@lancaster.ac.uk**; tel +44 1524 594691) or, for a local contact in North America, the US Office (**newphytol@ornl.gov**; tel +1 865 576 5261).